A&A 503, 207–211 (2009)
DOI: 10.1051/0004-6361/200811593

Astronomy & Astrophysics

Study of backward propagating and second harmonic Langmuir waves by 2D particle-in-cell simulation

Y. Huang[1,2] and G. L. Huang[1]

[1] Purple Mountain Observatory, Chinese Academy of Sciences, Nanjing 210008, Jiangsu, PR China
e-mail: huangyu@pmo.ac.cn
[2] Graduate University of Chinese Academy of Sciences, Beijing, PR China

Received 24 December 2008 / Accepted 19 May 2009

ABSTRACT

Context. Backward propagating and second harmonic Langmuir waves (LWs) play an important role in the second harmonic emission of solar radio type III bursts and they are numerically studied in detail with a new method.
Aims. We paid particular attention to the excitation mechanism of the backward propagating LWs, as well as the second harmonic LWs with two-dimensional (2D) particle-in-cell (PIC) simulations.
Methods. We performed simulations with two different types of initial conditions, i.e., the beam-exited and the wave-excited cases. In the second case, the beam-excited LWs were considered to represent the free energy instead of the beam itself.
Results. It is firstly found that the backward propagating LWs are suppressed by about 20% by the beam electrons. Hence, the beam electrons just have a negative contribution to the backward LWs, which can be explained in a preliminary way by the Landau damping of the beam electrons. On the other hand, the second harmonic LWs are contributed mainly (about 80%) by the beam electrons, only 20% originating from beam-excited forward LWs, which is quite different from earlier results.
Conclusions. Therefore, we found that the backward propagating LWs can't be amplified directly by the electron beam, and we must assume that they are generated by the beam-excited forward LWs scattered by ion sound waves. The direct amplification of beam-plasma instability may play an important role in producing the second harmonic LWs.

Key words. Sun: radio radiation – radiation mechanisms: general – methods: numerical

1. Introduction

Solar radio type III bursts have been intensively studied by both theory and observation, the latter of which may provide the most important diagnostics of electron acceleration with in solar flares. Energetic electrons accelerated in solar flares propagate along open magnetic field lines from solar corona to the interplanetary medium, and generate Langmuir waves (LWs) and the electromagnetic (EM) radiation of type III bursts, observed simultaneously by a series of spacecrafts (Lin et al. 1981; Reiner et al. 1992; Robinson et al. 1993; Hoang et al. 1994). It is widely accepted that the intensive LWs are generated at the electron plasma frequency ($f = f_p$) by the beam instability, i.e., the interaction between the ambient plasma and fast beam electrons. A part of the energy of LWs is converted into the EM radiation either at the fundamental ($f = f_p$), the second harmonic ($f = 2f_p$), or both. The second harmonic LWs and the EM emission are produced by the coalescence of two kinds of LWs, i.e., the forward and the backward propagating LWs, which are generated by the forward propagating LWs being scattered by the ion sound waves (Ginzburg & Zheleznyakov 1958; Bardwell & Goldman 1976; Robinson et al. 1988; Melrose 1991; Robinson et al. 1993; Cairns et al. 1995). Kasaba et al. (2001) performed PIC simulations by using one-dimensional (1D) and two-dimensional (2D) EM codes. In both of the 1D and 2D systems, the forward propagating LWs can be excited at $f = f_p$ and $f = 2f_p$, and the backward propagating LWs can be excited at $f = f_p$. The EM waves are produced at both $f = f_p$ and $f = 2f_p$ in the 2D system. The time evolution in the intensity of different plasma waves shows that the electrostatic (ES) LWs at $2f_p$ are correlated with the beam-excited LWs, while the EM waves at $2f_p$ are correlated with the backward propagating LWs. However, there is no correlation between the forward and backward propagating LWs, as well as the EM fundamentals.

In Huang & Huang (2007), we studied the dispersion relation of the backward propagation LWs with analytical and 1D PIC simulation methods. We also simulated the beam-plasma instability, and confirmed that the ions are necessary for increasing the backward propagating LWs. On the other hand, there are two kinds of free energy in plasma emission processes, i.e., the beam electrons and the beam-excited LWs. Both of them possibly contribute to the backward propagating LWs and the second harmonic LWs, in plasma emission processes. The main problem is in identifying which type of free energy is primarily responsible for the amplitude of these LWs. Hence, we performed 1D computer experiments with two different conditions, one the beam-plasma interaction, and the other the wave-plasma interaction (Huang & Huang 2008). We found that the electron beam is not really capable of generating the backward propagating LWs directly but may directly amplify the second harmonic LWs. However, these 1D results are only qualitative, so, in this paper we developed the 2D ES code be able to obtain quantitative results to compare with the 1D results.

The method of the 2D PIC simulations is introduced in Sect. 2. In Sect. 3, we present the beam-plasma interactions as the standard condition. In Sect. 4, we replace the beam electrons with the beam-excited LWs as the free energy. In Sect. 5, we

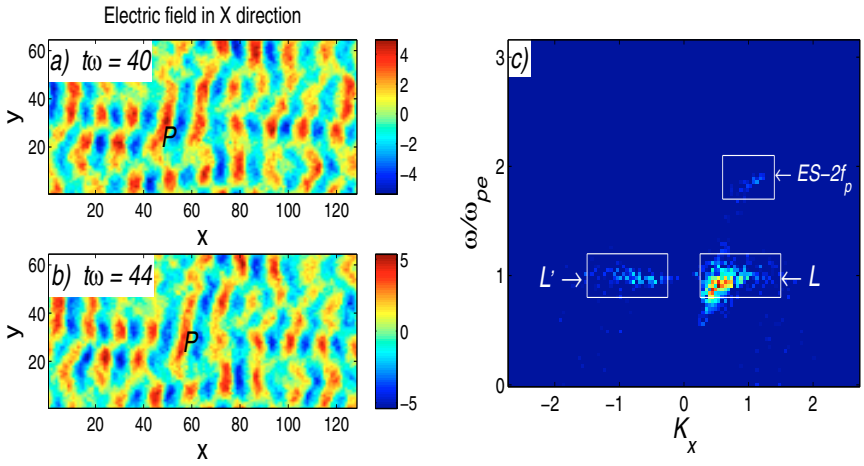

Fig. 1. **a)–b)** The electric field in the X-direction of the waves in $X-Y$ plane. **c)** The spectra obtained by Fourier transformation of the logarithm electric field in space along X-axis.

Table 1. The parameters of two dimensional simulation.

Parameters	Symbols	Simulation	Realistic scale
Number of time steps		4500	
Time step	Δt	0.01	
Timescale	$1/\omega_{\rm pe}$	0.25	1.6×10^{-5} s
Number of grid points	$N_x\times N_y$	128×64	
Grid spacing	$\triangle_x\triangle_y$	1	
Spatial scale	$c/\omega_{\rm pe}$	25	4.8×10^{3} m
Ambient Number of particles		16	
Beam Number of particles		4	
Ambient electron density	n	0.005	$1.24\times10^{6}m^{-3}$
Electron plasma frequency	$\omega_{\rm pe}$	4.0	10 kHz
Electron gyrofrequency	$\Omega_{\rm e}$	0.5	
Electron beam density	$n_{\rm b}$	0.025n	
Electron thermal velocity	$v_{\rm the}$	1	50 eV
Ion thermal velocity	$v_{\rm thi}$	0.005	2.3 eV
Ion mass	m_i	$1836m_{\rm e}$	
Speed of beam	$v_{\rm b}$	10	5 keV
Speed of light	c	100	3×10^{8} ms^{-1}

summarize and discuss the main results of this paper, as well as present future work that we intend to do.

2. Method of PIC simulations

We write an ES PIC code in a 2D system with a periodic boundary condition. The simulated system is located in an $X-Y$ plane, with an ambient magnetic field along the X-axis. The numbers of grid points are 128×64, and the grid dimensions $\triangle_x, \triangle_y$ both equal the electron Debye length ($\lambda_{\rm D}$). The time and spatial scales are normalized by $t_0 = 1/\omega_{\rm pe}$ and $x_0 = c/\omega_{\rm pe}$ ($\omega_{\rm pe} = 2\pi f_{\rm p}$), respectively. The mass and electricity scales are normalized by $m_0 = m_{\rm e}$ and $q_0 = e$, respectively. All parameters and their realistic values for the PIC simulations are listed in Table 1. These physical parameters (such as $n = 10^6\,{\rm m}^{-3}$) are very close to the natural plasma parameters in near-Earth space (Nicholson et al. 1978). In Table 1, the time, space, density, frequency, and energy are given in units of $\rm s, m, m^{-3}$, Hz, and eV, respectively. As for the initial condition, the ambient electrons and ions have Maxwellian distributions with electron and ion thermal velocities ($v_{\rm the}$ and $v_{\rm thi}$), respectively. The electron beam is injected along the ambient magnetic field with a velocity of $v_{\rm b}$, density of $n_{\rm b}$, and velocity broadness of $v_{\rm the}$. The simulations were performed with beam electrons, and ambient electrons and ions, for different values of $v_{\rm b}$ and $n_{\rm b}$. The ambient magnetic field is denoted by the electron cyclotron frequencies ($\Omega_{\rm e}$).

3. Standard case

We plot the electric field of the 2D simulations for the "standard" case of $t\omega_{\rm pe}\sim40$ and $t\omega_{\rm pe}\sim44$ in Figs. 1a and b. In the panels a and b, we can see that the peak of the same wave packet (marked by P) moves with time along the positive X direction, so, we can confirm that this wave is the forward LWs. However, the backward and second harmonic LWs are too weak to be directly seen in this figure. We can then derive the Fourier transform of the electric field of these waves as a function of both the coordinates of the X-axis in space and time, and obtain the corresponding spectra for them in Fig. 1c, which shows the $\omega-k_x$ diagram of the electric field along the ambient magnetic field. Therefore, we can clearly distinguish the forward and backward propagating LWs at $f = f_{\rm p}$, and the forward propagating LWs at $f = 2f_{\rm p}$, which are respectively denoted by L, L', and ES $-\,2f_{\rm p}$. The forward Langmuir wave-number in Fig. 1c occurs at the maximum linear growth rate at $k_x\sim\omega_{\rm pe}/v_{\rm b} = 0.4$, and the nonlinear stage starts at the beginning of the saturation phase of the beam instability at about $\omega_{\rm pe}t\approx40$ (Dum 1990). The apparent but weaker backward LWs also appear at k_x less than 0, with much slower growth than for the forward LWs. There are far weaker ES harmonic waves of forward LWs at frequencies near $\omega = 2\omega_{\rm pe}$. These features are generally comparable with the ones found in the previous PIC simulations (Nishikawa & Cairns 1991; Kasaba et al. 2001).

We then complete an additional analysis of these LWs in the three rectangles indicated in Fig. 1c. The time evolution in the different LWs are obtained by the reverse Fourier transform with in each area of L, L', and ES $-\,2f_{\rm p}$. As one example, we show the time evolution in the forward LWs in Fig. 2a. The black line indicates one peak of the forward LWs moving with time along the X direction. We can calculate the phase velocity of the forward LWs, which is given in Fig. 2a. The phase velocity of backward LWs or second harmonic LWs can be obtained by the same method. Figure 2b shows the relationship between the phase velocity of different LWs and the beam drift velocity. The phase velocity of forward LWs and second harmonic LWs have almost identical values, which are a little lower than the beam drift speed, and increase with increasing of beam drift speed. The velocity distribution function has a positive slope at a speed lower than the beam drift speed. The phase velocity of the LWs depends on this positive slope because of the wave-particle resonance. The velocity of the forward waves should therefore be a little lower than the beam drift speed. The phase velocity of backward LWs is also lower than the beam drift speed, with a very weak correlation between them.

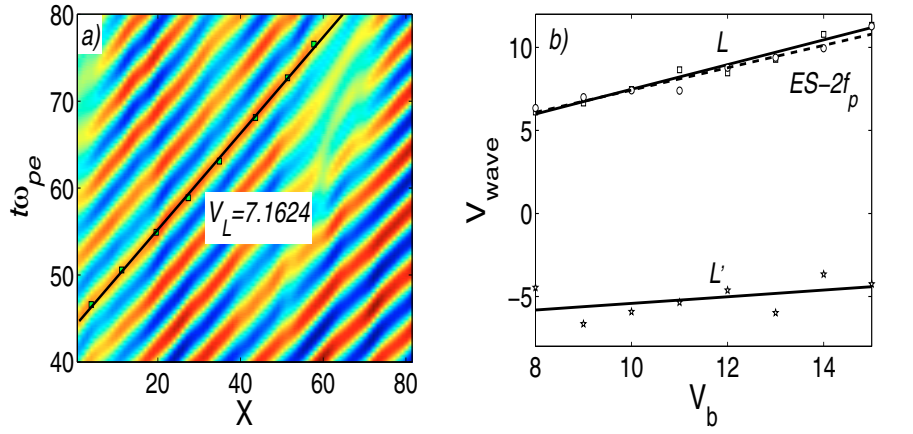

Fig. 2. **a)** The time evolution of the forward LWs. **b)** The phase velocity of different LWs versus the beam drift speed.

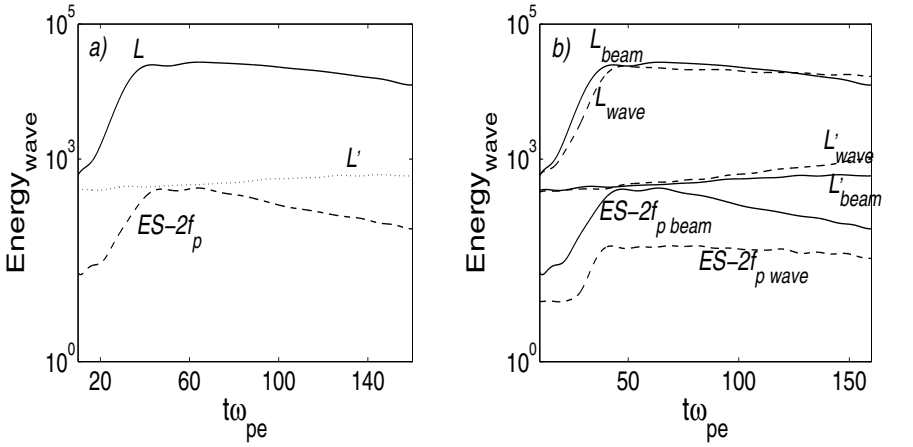

Fig. 3. **a)** Standard or beam-excited case, the forward, backward and second harmonic LWs are denoted by L (solid line), L' (dotted line) and ES $- 2f_p$ (dashed line), respectively. **b)** Wave-excited case (dashed lines) in comparison with those in the standard case (solid lines).

Moreover, we plot the evolution in the power density of different plasma waves in Fig. 3a, which shows that the forward propagating and second harmonic LWs are well correlated in their growing, saturation, and decay phases, and that they reach their maxima almost at similar times $t\omega_{pe} \sim 40$. The backward propagating LWs continuously grow till the end of the simulation with a very small growth rate. The energy ratio of the backward LWs to the forward LWs is about 1%, which is much smaller than the energy ratio (about 8%) of the forward LWs to the beam electrons. And the power of the ES second harmonic wave is usually a factor $10^{-2} \sim 10^{-3}$ that of the forward LWs. It is much larger than the values (about $10^{-4} \sim 10^{-5}$) excepted to be by the observations in the terrestrial electron foreshock and the plasma sheet boundary layer (see Fig. 3 in Kasaba et al. 2000).

The relative growth rate of different plasma waves in Fig. 3a is also defined $\omega_{i1} = (E(t_2) - E(t_1))/((N_2 - N_1)\mathrm{d}tE(t_1))$, where, E is the energy of the waves, the time interval between t_1 and t_2 is selected in the linearly growing phase, and N_1 and N_2 are the time steps for these two times. The relative growth rate is 0.206 for the forward LWs between $t\omega_{pe} \sim 29$ and $t\omega_{pe} \sim 36$, 0.191 for the second harmonic LWs from $t\omega_{pe} \sim 30$ to $t\omega_{pe} \sim 38$, and 0.0087 for the backward LWs from $t\omega_{pe} \sim 40$ to $t\omega_{pe} \sim 140$, respectively. Hence, the relative growth rates of the forward and second harmonic LWs are of the same order of magnitude, which is at least one order of magnitude larger than that of the backward propagating LWs.

We then perform 2D simulations with different parameters to compare the energies and growth rates of the plasma waves. Here, the wave energy is determined by its maximum value during the complete simulation times, and the growth rate is defined to be their absolute value, i.e., $\omega_{i2} = (E(t_2) - E(t_1))/((N_2 - N_1)\mathrm{d}t)$, to compare the growth rates of the same wave with different parameters. Figures 4a–d show the relationships of the wave energy and growth rates versus the beam density and the drift speed, respectively. In Fig. 4, both the energy and growth rates of the forward LWs and second harmonic LWs increase with increasing velocity and density of the beam electrons. The energy and growth rates of the backward LWs increase only with increasing beam velocity, but remain almost constant when the beam electron density increases, as we discuss below.

4. Wave-excited simulations

To quantitatively determine that the backward propagating LWs and the second harmonic LWs are amplified by the beam electrons directly or by the beam-excited LWs, we used the forward propagating LWs instead of the beam electrons as the free energy to excite the backward propagating LWs and the second harmonic LWs. Based on this "wave-excite" condition, all the energy in the generated backward and second harmonic LWs can originate only in the beam-excited forward LWs. In these wave-excited simulations, the drift speed of the beam electrons was set to be zero. In the first few steps, we defined the electric field of the beam-excited forward propagating LWs as the initial condition. Hence, the ambient electrons and ions moved both in the self-generated electric field and the electric field of the initial LWs. We controlled the initial LWs until the energy of electric field reached the energy of the beam-excited forward LWs (see Fig. 3b, the energy of L_{beam} and L_{wave} are almost same), to

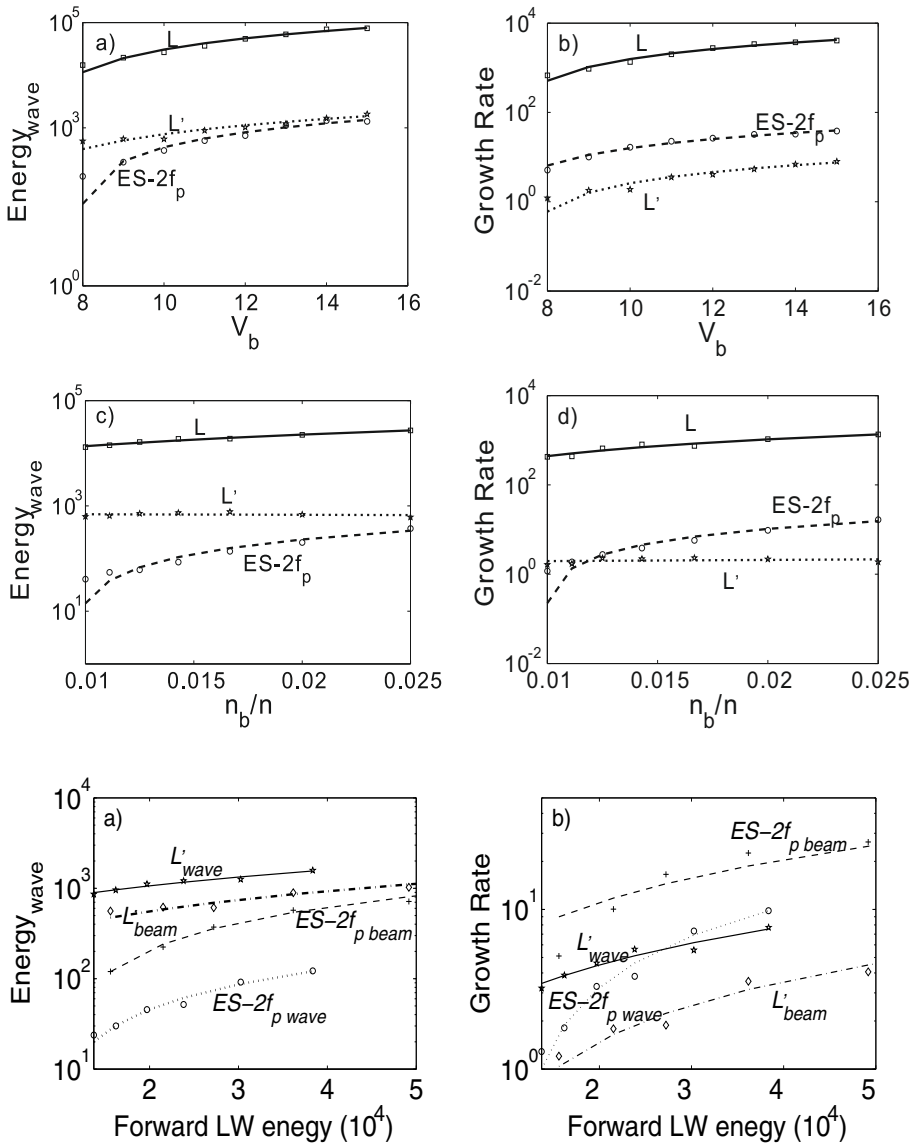

Fig. 4. Dependence of the power and growth rate of forward LWs, backward LWs, and second harmonic LWs on v_b and n_b. **a)** The relationship between the beam drift velocity and the energy. **b)** The relationship between the beam drift velocity and the growth rate. **c)** The relationship between the beam density and the energy. **d)** The relationship between the beam density and the growth rate. The speed of the beam electron varied from 8 to 15 (0.08c to 0.15c), and the beam density varied from 1% to 2.5%.

Fig. 5. The relationships between the maximum energy of the forward LWs and **a)** the maximum energy of the backward LWs (solid line) and the second harmonic LWs (dashed line), and **b)** the absolute growth rate of the backward LWs (solid line) and the second harmonic LWs (dashed line). The maximum energy and the absolute growth rate of the beam-excited backward LWs (dot-dashed line) and second harmonic LWs (dotted line) are added to the panels **a)** and **b)**, respectively.

obtain the backward propagating LWs and the second harmonic LWs evolved in the wave-excited simulations.

We also obtained the spectra of every Y line by obtaining a Fourier transform for the electric field in space along the X-axis and time. We then calculated the power of each wave by applying the reverse Fourier transform of every spectra. Figure 3b shows the time evolution in the power density of different plasma waves. The parameters of the wave-excited simulations are the same as those of beam-exited simulations in Table 1, except that the drift speed of beam electrons equals zero. The dashed and solid lines represent the energy of the wave-excited and beam-excited plasma waves, respectively.

In Fig. 3b, the energy of wave-excited second harmonic LWs is obviously lower than that of beam-excited ones, but the energy of the wave-excited backward propagating LWs is a little higher than that of beam-excited ones. Then, we controlled the amplitude of injected LWs to show the relationships between the maximum energy and absolute growth rate of the backward LWs, and between the second harmonic LWs and the maximum energy of the forward LWs in Fig. 5, in which all the curves represent the linear fit results. To compare the beam-excited and wave-excited cases, the results of the beam-excited plasma waves are also plotted in Fig. 5. The results in Fig. 5 confirm that the energy of the beam-excited second harmonic LWs is always higher than that of the wave-excited ones, The power ratio of the wave-excited second harmonic LWs to the beam-excited second harmonic LWs is about 20% when the power of beam-excited forward LWs is same. So, the beam energy is directly converted to the rest energy (80%) of second harmonic LWs, and the growth rate of second harmonic LWs in the beam-excited case is about one order of magnitude higher than that in the wave-excited case. The energy of beam-excited backward propagating LWs is always a little lower than that of wave-excited ones of the same power as beam-excited forward LWs. The power ratio of the wave-excited backward LWs to the beam-excited backward LWs is about 120%, while the absolute growth rate of the wave-excited backward LWs is about three times higher than that of the beam-excited ones.

5. Conclusions and discussion

We have performed numerical simulations with the ES particle code in a 2D periodic system to study the generation processes of the ES waves involved in the plasma emission mechanism of solar radio type III bursts. In particular, we have performed the simulations in the wave-excited condition to compare the

contributions of the electron beam and beam-excited LWs, as two distinguishable free energies for the backward LWs and second harmonic LWs. The main conclusions that we have reached are the following.

1) The energy of the wave-excited second harmonic LWs is obviously lower than that of the beam-excited ones, which imlies that the energy of the second harmonic LWs has been converted from that of both the beam electrons (about 80%) and beam-excited LWs (about 20%). The growth rate of second harmonic LWs in the beam-excited case is about one order of magnitude higher than that of the wave-excited case. Hence, the direct amplification of the beam electrons play a more important role for the second harmonic LWs, which is quite different from the earlier results mentioned in Sect. 1.

2) The energy of the wave-excited backward LWs is a little higher than that of the beam-excited ones, while the absolute growth rate of the wave-excited backward LWs is about three times higher than that of the beam-excited ones, which means that the backward LWs are mainly amplified by the beam-excited LWs, and the beam electrons just have a negative contribution (about 20%) for the backward LWs. We further suggest that the beam electrons may suppress the growth of purely wave-excited backward LWs by Landau damping (Chen 1980), i.e., $\mathrm{Im}\left(\frac{\omega}{\omega_\mathrm{p}}\right) = -0.22\sqrt{\pi}\left(\frac{\omega_\mathrm{p}}{kv_\mathrm{th}}\right)^3 \exp\left(\frac{-\omega_\mathrm{p}^2}{2k^2v_\mathrm{th}^2}\right)$, where, $\omega_\mathrm{p} = \sqrt{n_\mathrm{b}e^2/(m_\mathrm{e}\varepsilon)}$, n_b is the beam electron density. When ω_p varies from 1 kHz to 3 kHz the damping rate increases from −0.0129 to −0.1434. So, the Landau damping increases rapidly with the increasing density of the beam electrons, which may explain the small difference between the wave-excited and beam-excited backward LWs in Fig. 3b, as well as the reason why the energy and growth rate of backward LWs do not increase with beam density in Figs. 4c,d. However, Landau damping of the beam electrons does not depends on the beam speed, so, the energy and growth rates of backward LWs still increase with the increasing beam drift speed shown in Figs. 4a,b. We have confirmed the main results of the 1D PIC simulations that the electron beam is probably incapable of generating the backward LWs directly, and the energy of backward LWs originates in the beam-excited LWs, although the beam electrons may directly amplify the second harmonic LWs (Huang & Huang 2008). We also perform the simulations with different ambient magnetic fields ($\Omega_\mathrm{e}/\omega_\mathrm{pe} \approx 0.01 \sim 0.1$), all growth rates and energies of the three ES waves being subject to only little change. In our simulations, the direction of the magnetic field is the same as that of the beam drift. The magnetic field has a significant effect on the perpendicular waves, but was little effect on the parallel waves in our case. On the other hand, the magnetic field which (varied from 0.01 to 0.1) represents the weak magnetic field case. Such a weak field will not affect the instability of high frequency waves such as LWs (Dum & Nishikawa 1994). Hence, the ambient magnetic field evidently does not affect the properties of ES waves in our simulations.

On the other hand, a series of questions remain unanswered about the plasma radiation mechanism from observations of present spacecrafts (e.g., WIND and ULYSSES). For example, only a small set of type III bursts drift downward close to the local plasma frequency. The low-frequency cutoff of type III bursts is strongly suggested to be an intrinsic property of the radiation mechanism, which seems to be a new challenge for the classical model of plasma radiation (Leblanc et al. 1995). Therefore, it is necessary to study the relationships between the electron beam and the relevant ES and EM plasma waves very carefully. We intend to study the properties of the EM plasma waves in type III bursts with 2D EM PIC simulations to identify whether the energy of type III bursts originates in the beam electrons directly or in energy converted from the beam-excited LWs.

Acknowledgements. This study is supported by the NFSC projects with Nos. 10773032, and 10833007, and "973" program with No. 2006CB806302. The authors would like to thank Dr. Melnikov, V. F. and other solar radio colleague for helpful discussions.

References

Bardwell, S., & Goldman, M. V. 1976, ApJ, 209, 912
Cairns, I. H., & Robinson, P. A. 1995, Geophys. Res. Lett., 22, 3437
Chen, F. F. 1980, Introduction to Plasma Physics, 141
Dum, C. T. 1990, J. Geophys. Res., 95, 8095
Dum, C. T., & Nishikawa, K. I. 1994, Phys. Plasmas, 1, 1821
Ginzburg, V. L., & Zheleznyakov, V. V. 1958, Sov. Astron., 2, 653
Hoang, S., Dulk, G. A., & Leblanc, Y. 1994, A&A, 289, 957
Huang, Y., & Huang, G. L. 2007, Acta Astron. Sinica, 48 441; 2008, Chinese Astron. Astrophys., 32, 178
Huang, Y., & Huang, G. L. 2008, Adv. Space Res., 41, 1202
Kasaba, Y., Matsumoto, H., Omura, Y., et al. 2000, J. Geophys. Res., 105, 79
Kasaba, Y., Matsumoto, H., & Omura, Y. 2001, J. Geophys. Res., 106, 18693
Leblanc, Y., Hoang, S., & Dulk, G. A. 1995, Geophys. Res. Lett., 22, 3429
Lin, R. P., Potter, D. W., Gurnett, D. A., & Scarf, F. L. 1981, ApJ, 251, 364
Melrose, D. B. 1991, Annu. Rev. Astron. Astrophys., 29, 31
Nicholson, D. R., Goldman, M. V., Hoyng, P., & Weatherall, J. C. 1978, ApJ, 223, 605
Nishikawa, K. I., & Cairns, I. H. 1991, J. Geophys. Res., 96, 19343
Reiner, M. J., Stone, R. G., & Fainberg, J. 1992, ApJ, 394, 340
Robinson, P. A., Newman, D. L., & Goldman, M. V. 1988, Phys. Rev. Lett., 61, 702
Robinson, P. A., Cairns, I. H., & Gurnett, D. A. 1993, ApJ, 407, 790